# A Finite Difference Approach that Employs an Asymptotic Boundary Condition on a Rectangular Outer Boundary for Modeling Two-Dimensional Transmission Line Structures

Richard K. Gordon, *Member, IEEE,* and Set Hin Fook

***Abstract*— In this paper, the derivation of three asymptotic boundary conditions is presented. Techniques for implementing each of these on finite difference meshes with rectangular outer boundaries are discussed. Numerical results obtained using these boundary conditions in the finite difference analysis of both shielded and unshielded transmission lines are shown. We present detailed convergence studies on the use of each of these boundary conditions and discuss the memory requirements of each.**

## I. Introduction

BECAUSE of its great importance in the design of integrated microwave circuit components, the problem of determining the coefficients of capacitance of a multiconductor microstrip transmission line has received a great deal of attention in the literature. See, for instance, [1]–[5]. Among the methods that have been used are the finite element method [1], the semi-discrete finite element method [2], the spectral Green's function approach [3], integral equation approaches [4]–[5], and others. In this paper, we present a finite difference approach for solving this problem. This method can be used in the analysis of structures having microstrip lines of either zero or nonzero thickness and either planar or nonplanar dielectric interfaces. In order to solve the problem with as few unknowns as possible, we use a finite difference mesh having a rectangular outer boundary. Using a method that is similar to that presented by Mittra and Ramahi in [6], we derive three asymptotic boundary conditions (ABC's) that can be used with such a mesh and present a detailed convergence study of each.

## II. Derivation of Boundary Conditions

Our goal is to develop boundary conditions that can be used in problems such as that depicted in Fig. 1; a finite difference mesh with a rectangular outer boundary encloses a structure consisting of microstrip lines residing on a grounded dielectric substrate. In a charge-free region, the electric potential $v$ behaves as

$$v(\rho,\phi) = C_0 + A_0(\phi)\ln\rho + \sum_{n=1}^{\infty}\frac{A_n(\phi)}{\rho^n} \tag{1}$$

Manuscript received July 2, 1992; revised October 26, 1992.

R. K. Gordon is with the Department of Electrical Engineering, University of Mississippi, University, MS 38677.

S. H. Fook is with Gravel Equipment & Supply, Inc., Amory, MS.

IEEE Log Number 9208340.

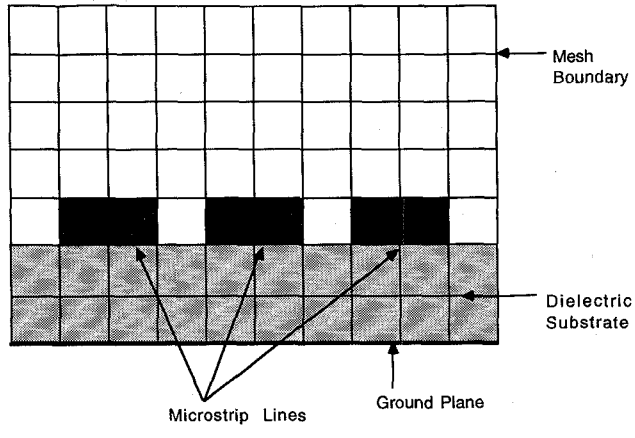


Fig. 1. Diagram of problem.

where $\rho = (x^2+y^2)^{1/2}$ and $\phi = \tan^{-1}(y/x)$. The charge on the microstrip lines is balanced by image charge on the ground plane. Thus, the total charge enclosed by the finite difference mesh is zero. So, $A_0$ must be zero. Furthermore, because the ground plane is at zero potential and extends to infinity, $C_0$ must be zero as well. So, the equation describing the behavior of $v$ at the outer boundary of the finite difference mesh is

$$v(\rho,\phi) = \frac{A_1(\phi)}{\rho} + \frac{A_2(\phi)}{\rho^2} + \frac{A_3(\phi)}{\rho^3} + \cdots. \tag{2}$$

One of the most widely used boundary conditions in problems such as this, the shield boundary condition, states that $v = 0$ along the outer boundary of the mesh. As will be demonstrated in Section IV, this is an approximate boundary condition which becomes more accurate as the outer boundary of the mesh is moved further away from the center of charge. For each of the ABC's we will derive, we will arrive at an equation similar to (2), and will then argue that for sufficiently large values of $\rho$, the higher order terms on the right-hand side make a negligible contribution to the sum and can therefore be dropped from the equation. At this point, we note that the shield boundary condition can be viewed in the same light; that is, the shield boundary condition can be considered to be a lowest order ABC in which all of the terms on the right-hand side of (2) have been discarded. For this reason,

and for the sake of convenience, we will refer to the shield boundary condition as ABC0 in the remainder of this paper. We now proceed to the derivation of the next lowest order ABC, which will henceforth be referred to as ABC1. The treatment is similar to that presented by Mittra and Ramahi in [6].

If (2) is differentiated with respect to $\rho$ and the resulting equation is added to $1/\rho$ times (2), we arrive at the equation

$$\frac{\partial v}{\partial \rho} + \frac{1}{\rho} v = -\frac{A_2}{\rho^3} - \frac{2A_3}{\rho^4} - \frac{3A_4}{\rho^5} - \frac{4A_5}{\rho^6} - \cdots. \tag{3}$$

We obtain ABC1 by setting the right-hand side of this equation to zero, an approximation which, as will be demonstrated by the numerical results, becomes increasingly accurate as the outer boundary of the mesh is moved away from the center of charge. Note that for large values of $\rho$, the error incurred by dropping the right-hand side of (2) to obtain ABC0 is proportional to $(1/\rho)^1$, while that incurred by dropping the right-hand side of (3) to obtain ABC1 is proportional to $(1/\rho)^3$. Thus, ABC1 is of higher order than ABC0, and would therefore be expected, in general, to be more accurate. This will be investigated further in Section IV.

In order to obtain a boundary condition of still higher order, which we will designate as ABC2, we differentiate (3) with respect to $\rho$ and add the resulting equation to $3/\rho$ times (3). The result is

$$\frac{\partial^2 v}{\partial \rho^2} + \frac{4}{\rho}\frac{\partial v}{\partial \rho} + \frac{2}{\rho^2} v = \frac{2A_3}{\rho^5} + \frac{6A_4}{\rho^6} + \frac{12A_5}{\rho^7} + \cdots. \tag{4}$$

If we use Laplace's equation to rewrite $v_{\rho\rho}$ in terms of $v_\rho$ and $v_{\phi\phi}$, the resulting equation is

$$\frac{3}{\rho}\frac{\partial v}{\partial \rho} + \frac{2}{\rho^2} v - \frac{1}{\rho^2}\frac{\partial^2 v}{\partial \phi^2} = \frac{2A_3}{\rho^5} + \frac{6A_4}{\rho^6} + \frac{12A_5}{\rho^7} + \cdots. \tag{5}$$

We obtain ABC2 by dropping the right-hand side of this equation; for large values of $\rho$, the error incurred by making this approximation is proportional to $(1/\rho)^5$. So, indeed, ABC2 is of higher order than ABC0 or ABC1.

## III. Numerical Implementation of Boundary Conditions

The mathematical expressions for ABC0, ABC1, and ABC2 are

ABC0:

$$v = 0 \tag{6}$$

ABC1:

$$\frac{\partial v}{\partial \rho} = -\frac{1}{\rho} v \tag{7}$$

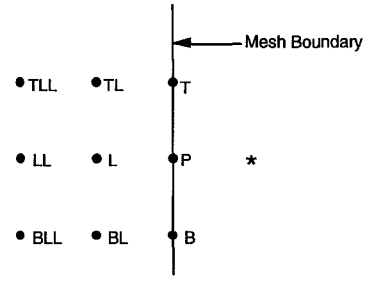


Fig. 2. Diagram for mesh truncation.

ABC2:

$$\frac{\partial v}{\partial \rho} = -\frac{2}{3\rho} v + \frac{1}{3\rho}\frac{\partial^2 v}{\partial \phi^2}. \tag{8}$$

In the numerical solution of this problem, we enforce the appropriate Dirichlet boundary condition at each node residing on a conducting surface and the continuity of the normal component of the electric flux density at nodes located on dielectric interfaces. At interior nodes, we enforce the finite difference representation of Laplace's equation, which is written in terms of the value of $v$ at the node itself and at each of the four surrounding nodes. But, for nodes on the outer boundary of the mesh, the imposition of Laplace's equation poses a difficulty; there are not four surrounding nodes. we must find either another equation to enforce or some other way of applying Laplace's equation. With ABC0, we take the former alternative; we simply enforce the equation $v = 0$ at the outer boundary of the mesh. With ABC1 and ABC2, we pursue the second option; we use the ABC to find the normal derivative of the unknown at the outer boundary of the mesh. This normal derivative is then used to write the value of the potential just outside the mesh in terms of the potential at nodes near the outer boundary. Once this has been done, Laplace's equation can be enforced. Thus, we must now show how (7) and (8) can be used to find the normal derivative of the unknown at the outer boundary of the mesh.

In Fig. 2, $P$ is a node on the right-hand side of the rectangular outer boundary; $T, B, TL, L, BL, TLL, LL$, and $BLL$ are surrounding nodes. The position marked * is outside the mesh; as a result of this, Laplace's equation cannot be enforced at $P$ in the usual way. Our goal is to express the potential at * in terms of the potential at $P$ and the surrounding nodes; once this has been done, Laplace's equation can be enforced at $P$. In order to achieve this goal, we must obtain information about the normal derivative of the potential at node $P$. That is, we must find $v_x(P)$. In the application of ABC1, this is rather simple. We use the chain rule and the relationship between cylindrical and Cartesian coordinates to rewrite (7) as

$$\frac{\partial v}{\partial x} = -\frac{1}{x}\left(v + y\frac{\partial v}{\partial y}\right). \tag{9}$$

The finite difference approximation for $v_x(P)$ is

$$\frac{\partial v}{\partial x}(P) = \frac{v(*) - v(L)}{x(*) - x(L)} = \frac{v(*) - v(L)}{2\Delta}. \tag{10}$$

If (9) is substituted into (10), we obtain

$$v(*) = v(L) - \frac{2\Delta}{x(P)} \cdot \left[ v(P) + y(P)\frac{\partial v}{\partial y}(P) \right]. \tag{11}$$

When the finite difference approximation for $v_y(P)$, which is the same as the right-hand side of (10) except that $*, L$, and $x$ are replaced by $T, B$, and $y$, respectively, is substituted into (11), the result is

$$v(*) = C_L v(L) + C_P v(P) + C_T v(T) + C_B v(B) \tag{12}$$

where

$$C_L = 1$$

$$C_P = -\frac{2\Delta}{x(P)} \cdot \frac{3y^2(P) - 2y(P)\,y(B) - 2y(P)\,y(T) + y(T)\,y(B)}{(y(P) - y(T))(y(P) - y(B))}$$

$$C_T = -\frac{2\Delta}{x(P)} \frac{y^2(P) - y(B)\,y(P)}{(y(T) - y(P))(y(T) - y(B))}$$

$$C_B = -\frac{2\Delta}{x(P)} \frac{y^2(P) - y(T)\,y(P)}{(y(B) - y(P))(y(B) - y(T))}.$$

Equation (12) represents the method of numerical implementation of ABC1 on the right-hand side of a rectangular outer boundary. It expresses $v(*)$ in terms of the values of $v$ at $P, T, L$, and $B$. So, Laplace's equation can now be enforced at $P$. A similar method is used on the left-hand side and top of the outer boundary.

Note that this method of mesh truncation does not increase the bandwidth of the finite difference matrix. Thus, the use of ABC1 requires no more computer memory than does the use of ABC0.

Finding a convenient expression for the normal derivative of $v$ at $P$ is somewhat more involved when ABC2 is used. We first use the chain rule to rewrite (8) as

$$\frac{\partial v}{\partial x}(P) = \frac{1}{(1+\beta\rho)\cos\phi} \cdot \left[ \alpha v - \frac{\partial v}{\partial y}(1+\beta\rho)\sin\phi + \beta\rho^2 \sin^2\phi \frac{\partial^2 v}{\partial x^2} + \beta\rho^2 \cos^2\phi \frac{\partial^2 v}{\partial y^2} - 2\beta\rho^2 \sin\phi\cos\phi \frac{\partial^2 v}{\partial x \partial y} \right] \tag{13}$$

where $\alpha = -2/3\rho$ and $\beta = 1/3\rho$.

Substitution of (13) into (10) yields

$$v(*) = v(L) + \frac{2\Delta}{(1+\beta\rho)\cos\phi} \cdot \left[ \alpha v(P) - \frac{\partial v(P)}{\partial y}(1+\beta\rho)\sin\phi + \beta y^2(p)\frac{\partial^2 v(P)}{\partial x^2} + \beta x^2(P)\frac{\partial^2 v(P)}{\partial y^2} - 2\beta x(P)\,y(P)\frac{\partial^2 v(p)}{\partial x \partial y} \right]. \tag{14}$$

In (14), the goal of expressing $v(*)$ in terms of the values of $v$ at $P$ and the surrounding nodes has been nearly achieved; the only remaining difficulty is the presence of the mixed derivative term. We present a novel approach for the evaluation of this term; the method is simple and, as will be shown Section IV, yields accurate results even when the outer boundary is quite close to the microstrip lines. We begin by defining $f(x,y)$ by the equation $f(x,y) = v_y(x,y)$. Thus, $v_{xy} = f_x$. So, if we can find $f_x$ at $P$ in terms of the values of $v$ at $P$ and the surrounding nodes, we can substitute the result into (14) and obtain a convenient expression for mesh truncation. The way we do this is to employ a second-order accurate, one-sided derivative formula for $f_x$ at $P$. This formula is

$$f_x(P) = Af(P) + Bf(L) + Cf(LL). \tag{15}$$

where

$$A = \frac{(2x(P) - x(L) - x(LL))}{(x(P) - x(L))(x(P) - x(LL))},$$

$$B = \frac{(x(P) - x(LL))}{(x(L) - x(P))(x(L) - x(LL))}$$

$$C = \frac{(x(P) - x(L))}{x(LL) - x(P))(x(LL) - x(L))}.$$

Recall that in (15), $f_x(P) = v_{xy}(P), f(P) = v_y(P), f(L) = v_y(L)$, and $f(LL) = v_y(LL)$. If we make these substitutions in (15), substitute the resulting expression for $v_{xy}(P)$ into (14), use Laplace's equation to rewrite $v_{xx}$ in (14) in terms of $v_{yy}$, and then use the finite difference approximations for all derivatives with respect to $y$, we obtain

$$v(*) = C_L v(L) + C_P v(P) + C_T v(T) + C_B v(B) + C_{LL} v(LL) + C_{TL} v(TL) + C_{BL} v(BL) + C_{TLL} v(TLL) + C_{BLL} v(BLL) \tag{16}$$

where $C_L, C_P, C_T, C_B, C_{LL}, C_{TL}, C_{BL}, C_{TLL}$, and $C_{BLL}$ are shown at the bottom of the next page.

Equation (16) represents the method of numerical implementation of ABC2 on the right-hand side of a rectangular outer boundary. It expresses $v(*)$ in terms of the values of $v$ at $P$ and the surrounding nodes. So, Laplace's equation can now be enforced at node $P$, which is on the right-hand side of the ouer boundary. A similar approach is used on the left-hand side and top of the outer boundary. This method of mesh truncation will, in general, increase the bandwidth of the finite difference matrix.

The only remaining question is the method used for mesh truncation at the two upper corners of the mesh. The method, which was used in both ABC1 and ABC2, is illustrated in Fig. 3, which shows the upper right corner of the mesh. (The spacing between the nodes in this figure has been greatly exaggerated for the sake of clarity.) At the corner point $P$, an interpolation method is used to write $v(P)$ in terms of the values of $v$ at points $B$ and $L$. We begin by noting that since $\rho$ achieves its maximum value at the corners of the mesh, the

contribution made by the higher order terms to the summation appearing on the right-hand side of (2) will be smaller at the corners of the mesh than at any other nodes. For this reason, and in order to avoid any further increase in the bandwidth of the finite difference matrix, we retain only the first term of the right-hand side of (2) in the mesh truncation technique we use at the corners. Thus, in the vicinity of the corner, we have $A_1(\phi) = v(\rho, \phi)\rho$. Using linear interpolation, we write the value of $A_1$ at $\phi(P)$ in terms of its value at $\phi(B)$ and $\phi(L)$ as

$$A_1(\phi(P)) = A_1(\phi(B)) + \frac{A_1(\phi(L)) - A_1(\phi(B))}{\phi(L) - \phi(B)}(\phi(P) - \phi(B)). \tag{17}$$

Since $A_1(\phi) = v(\rho, \phi)\rho$ near the corner, this becomes

$$\rho(P)\, v(P) = \rho(B)\, v(B) + \frac{\rho(L)\, v(L) - \rho(B)\, v(B)}{\phi(L) - \phi(B)}(\phi(P) - \phi(B)). \tag{18}$$

After (18) is rearranged, we obtain

$$v(P)\,\rho(P) + v(B)\left[\rho(B)\frac{\phi(P) - \phi(L)}{\phi(L) - \phi(B)} + v(L)\left[-\rho(L)\frac{\phi(P) - \phi(B)}{\phi(L) - \phi(B)}\right] = 0\right. \tag{19}$$

where $\rho(P) = (x(P)^2 + y(P)^2)^{1/2}$ and $\phi(P) = \tan^{-1}(y(P)/x(P))$.

This is the equation that is enforced at the upper right corner of the mesh. A similar equation is enforced at the upper left corner.

As was mentioned above, for a given mesh, the use of ABC2 will require more memory than will the use of ABC0 or ABC1. As we will now show, for unshielded structures, this disadvantage is more than compensated for by the fact that ABC2 allows the accurate solution of the microstrip problem with a much smaller mesh than that required by ABC0 or ABC1.

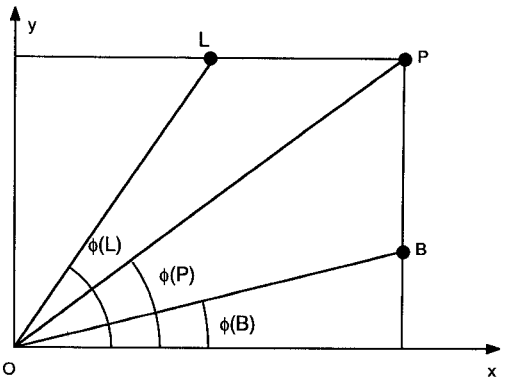


Fig. 3. Mesh truncation at corner.

## IV. Numerical Results

We present numerical results for two problems. The first is depicted in Fig. 4. Two 3 mil × 1 mil conductors are located in the free space region between two grounded planes. The bottom surface of each conductor is 1 mil above the lower ground plane, while the top surface is 3 mil below the upper one. The separation between the conductors is 2 mil. We use the finite difference method to find the coeficients of capacitance. We use a mesh density of 225 nodes/mil$^2$. The mesh is truncated at a distance $D$ to the left of the left conductor and $D$ to the right of the right conductor. The ABC is enforced along these two vertical sides. The coefficients of capacitance are determined first using ABC0, then ABC1, and finally ABC2. The value of $D$ is then increased and the procedure is repeated. The numerical results are recorded in Figs. 5 and 6. In the above derivations, it was predicted that for each of the ABC's, the numerical solution would converge to the actual solution as the outer boundary of the mesh is moved away from the center of charge. In Figs. 5 and 6, we see that this is indeed the case. The final value for $C_{11}$ is 1.623 pF/in; for $C_{12}$, it is $-0.151$ pF/in. (The numerically determined values for $C_{21}$ and $C_{22}$, respectively, were, as expected, identical to the values obtained for $C_{12}$ and $C_{11}$.) Weeks [4] analyzed this same structure; his values for $C_{11}$ and $C_{12}$, respectively, are 1.608 and $-0.150$ pF/in. The differences between the values obtained using the finite difference approach and those obtained by Weeks are 0.933%

$$C_L = 1 + \gamma(\beta y(P)^2 GG - 2\beta x(P)\, y(P) BD)$$
$$C_P =, \gamma[\alpha - D(1 + \beta\rho)\,\sin\,\phi + \beta y(P)^2 G + \beta x(P)^2 H - 2\beta x(P)\, y(P) AD]$$
$$C_T = \gamma[-E(1 + \beta\rho)\,\sin\,\phi + \beta x(P)^2 HH - 2\beta x(P)\, y(P) AE]$$
$$C_B = \gamma[-F(1 + \beta\rho)\,\sin\,\phi + \beta x(P)^2 HHH - 2\beta x(P)\, y(P) AF]$$
$$C_{LL} = \gamma[\beta y(P)^2 GGG - 2\beta x(P)\, y(P) CD]$$
$$C_{TL} = \gamma[-2\beta x(P)\, y(P) BE]$$
$$C_{BL} = \gamma[-2\beta x(P)\, y(P) BF]$$
$$C_{TLL} = \gamma[-2\beta x(P)\, y(P) CE]$$
$$C_{BLL} = \gamma[-2\beta x(P)\, y(P) CF].$$

TABLE I
NUMBER OF ENTRIES IN BANDED MATRIX FOR FIRST NUMERICAL CASE

| D(mils) | ABC0 | ABC1 | ABC2 |
|---|---|---|---|
| 0.133 | 2,175,500 | 2,175,500 | 4,370,000 |
| 0.267 | 2,245,116 | 2,245,116 | 4,509,840 |
| 0.400 | 2,314,732 | 2,314,732 | 4,649,680 |
| 0.533 | 2,384,348 | 2,384,348 | 4,789,520 |
| 0.733 | 2,488,772 | 2,488,772 | 4,999,280 |
| 1.000 | 2,628,004 | 2,628,004 | 5,278,960 |
| 1.333 | 2,802,044 | 2,802,044 | 5,628,560 |
| 2.000 | 3,150,124 | 3,150,124 | 6,327,760 |
| 3.000 | 3,672,244 | 3,672,244 | 7,376,560 |
| 4.000 | 4,194,364 | 4,194,364 | 8,425,360 |
| 5.000 | 4,716,484 | 4,716,484 | 9,474,160 |

TABLE II
NUMBER OF ENTRIES IN BANDED MATRIX FOR SECOND NUMERICAL CASE

| D(mils) | ABC0 | ABC1 | ABC2 |
|---|---|---|---|
| 0.300 | 509,124 | 509,124 | 1,025,904 |
| 0.500 | 581,854 | 581,854 | 1,172,080 |
| 0.700 | 661,200 | 661,200 | 1,331,520 |
| 1.000 | 793,254 | 793,254 | 1,596,810 |
| 1.400 | 995,170 | 995,170 | 2,002,330 |
| 2.500 | 1,720,554 | 1,720,554 | 3,458,400 |
| 3.500 | 2,628,004 | 2,628,004 | 5,278,960 |
| 4.500 | 3,808,854 | 3,808,854 | 7,647,120 |
| 5.500 | 5,299,104 | 5,299,104 | 10,634,880 |
| 6.000 | 6,171,504 | 6,171,504 | 12,383,610 |
| 8.000 | 10,614,604 | 10,614,604 | |
| 9.000 | 13,471,254 | 13,471,254 | |

for $C_{11}$ and 0.667% for $C_{12}$. In Section II, we predicted that, for a given mesh size, the results obtained using ABC2 would be more accurate than those obtained using ABC1, which would, in turn, be more accurate than those obtained using ABC0. This prediction is also verified. In fact, when ABC2 is used, even when $D$ is as small as 0.133 mil, the value for $C_{11}$ differs from the final converged value by only 4.067%, and the value for $C_{12}$ differs from its final value by 0.662%. To obtain this same degree of accuracy in $C_{11}$ and $C_{12}$ using ABC1, $D$ must be at least 1.333 mil; using ABC0, $D$ must be at least 2.0 mil. Recall, however, that while the use of ABC0 or ABC1 does not increase the bandwidth of the finite difference matrix, the use of ABC2 does. The effect this has on the total number of entries in the banded matrix is shown in Table I. This table shows the total number of entries in the banded matrix for each of the boundary conditions for each value of $D$. We note that for a given value of $D$, the amount of memory required by ABC1 is the same as that required by ABC0, while that required by ABC2 is twice as much. But, as we have just mentioned, in order to achieve the same degree of accuracy with ABC1 as that obtained using ABC2, a larger value of $D$ must be used; and to achieve this with ABC0, it must be made larger still. The number of entries in the banded matrix when ABC2 is used at $D = 0.133$ mil is 4 370 000. The same degree of accuracy is obtained using ABC1 at $D = 1.333$ mil; the number of entries in the banded matrix for this computation is 2 802 000. If we use ABC0 at $D = 2.0$, the number of entries is 3 150 124. Thus, for this case of a structure that is completely shielded above and below, the extra cost of using ABC2 is not justified; the problem can be solved more economically using ABC1 or even ABC0. The reason for this is that, for this case of a structure that is bounded above and below, the number of unknowns increases only linearly with $D$. Thus, even though the value of $D$ that must be used to obtain reasonable results using ABC1 is quite a bit larger than that required when ABC2 is used, the fact that ABC2 doubles the bandwidth of the finite difference matrix makes ABC1 preferable to ABC2. But for the case of an unshielded structure, the situation is quite different.

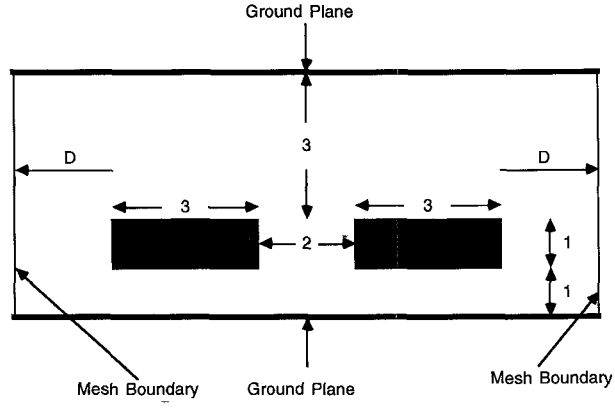


Fig. 4. Shielded transmission line for first numerical case.

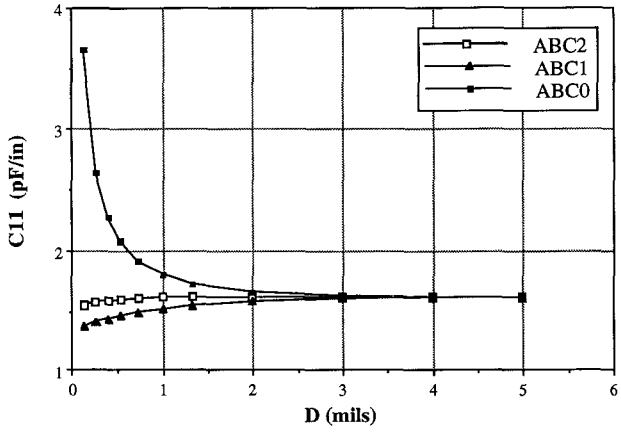


Fig. 5. Numerical value obtained for $C_{11}$ as a function of $D$.

The second structure we consider is shown in Fig. 7. The geometry is the same as that considered in the first case, except that the upper ground plane has been removed and a dielectric substrate of relative permittivity 2.0 has been placed under the conductors. Again, since $C_{12} = C_{21}$ and, for this geometry, $C_{11} = C_{22}$, we present results only for $C_{11}$ and

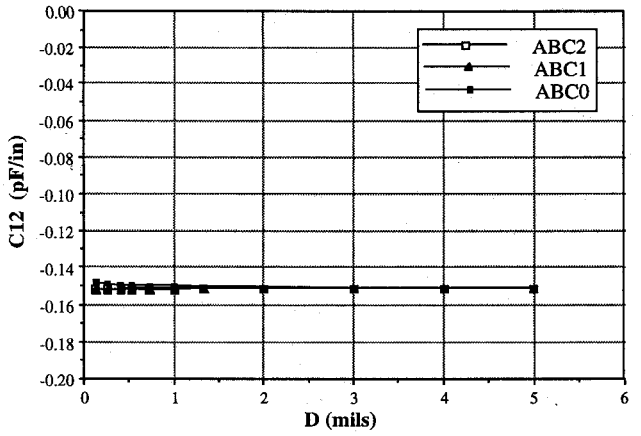


Fig. 6. Numerical value obtained for $C_{12}$ as a function of $D$.

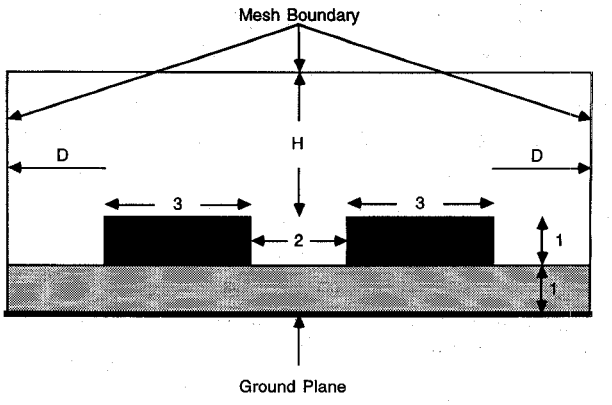


Fig. 7. Unshielded transmission line for second numerical case.

$C_{12}$. The procedure we employ in this problem differs from that followed in the first case in three respects. First, since the upper ground plane has been removed, we must apply an ABC on the top of the mesh as well as on the sides. Second, numerical experiment has shown that in order to obtain accurate results for both $C_{11}$ and $C_{12}$, it is insufficient to increase just $D$ or $H$ alone. Both must be moved away from the center of charge. So, as we increased $D$, we increased $H$ by the same amount, always maintaining $H$ at the value of $D+2$. Note that this means that the number of nodes in the mesh will increase as the square of $D$ as the mesh is enlarged. The final difference from the procedure we employed in the first problem is that we now use a mesh density of 100 nodes/mil$^2$. This lowered mesh density was employed so that relatively large values of $D$ could be used without exceeding the permitted storage of the computer. Even then, the results for ABC0, which are shown along with the results for ABC1 and ABC2 in Table II and Figs. 8 and 9, never completely converged before the memory capacity of the computer was reached. The value for $C_{11}$ has converged; that for $C_{12}$ is clearly doing so as well, but has not yet reached its final value. For ABC1 and ABC2, the values for both $C_{11}$ and $C_{12}$ have converged. The final value for $C_{11}$ is 2.378 pF/in; for $C_{12}$, it is $-0.219$ pF/in. The results obtained by Weeks [4] are 2.372 pF/in for $C_{11}$ and $-0.218$ pF/in for $C_{12}$. The differences between the values obtained using the finite difference approach and those obtained by Weeks are 0.253% for $C_{11}$ and 0.459% for $C_{12}$. The value obtained for $C_{11}$ using ABC2 at $D = 0.3$ mil differs from the final value by 0.0841%; for $C_{12}$, the difference is 2.283%. This calculation using ABC2 at $D = 0.3$ mil required the storage of a banded matrix having 1 025 903 entries. To achieve the same accuracy with ABC1, $D$ must be at least 4.5 mil. This computation required a banded matrix with 3 808 854 entries. Thus, the amount of storage required is almost four times that required when ABC2 is used. If ABC0 is used, even when $D = 9.0$ mil and the number of entries in the banded matrix is 13 471 254, the results obtained are not as accurate as those obtained using ABC2 at $D = 0.3$ mil. Clearly, for this unshielded problem, ABC2 is superior to ABC1 or ABC0. With ABC2, impressive accuracy can be obtained using a banded matrix with as few as 1 million entries.

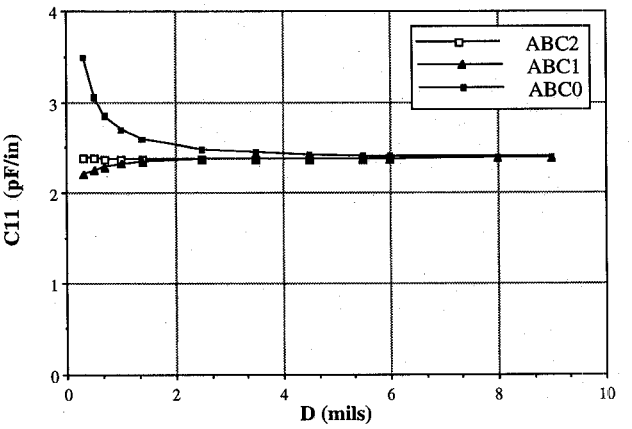


Fig. 8. Numerical value obtained for $C_{11}$ as a function of $D$.

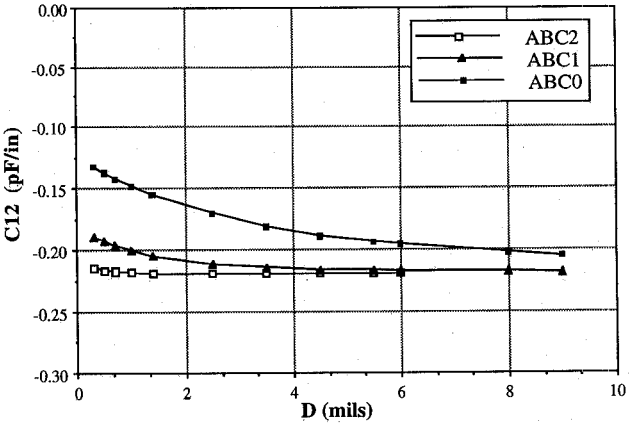


Fig. 9. Numerical value obtained for $C_{12}$ as a function of $D$.

## V. Conclusions

In this paper, we have presented the derivation of three asymptotic boundary conditions. We have shown how these boundary conditions can be implemented numerically, and have presented detailed convergence studies of their use. We have seen that for a given mesh, ABC2 is more accurate than ABC1, which, in turn, is more accurate than ABC0. Since ABC1 requires no more storage than ABC0, this increased accuracy means that, in terms of memory, ABC1 is always preferable to ABC0. Because ABC2 doubles the bandwidth of

the finite difference matrix, in some cases where the number of nodes increases slowly as the mesh is enlarged, ABC1 might be preferable to ABC2 even though its use requires a larger mesh. But for an unshielded structure, ABC2 is clearly the best choice. This boundary condition is simple to implement numerically and yields consistently accurate results. It appears to be an attractive option for the truncation of finite difference meshes used in the analysis of unshielded transmission lines.

## REFERENCES


[1] A. Khebir, A. B. Kouki, and R. Mittra, "Higher order asymptotic boundary condition for the finite element modeling of two-dimensional transmission line structures," *IEEE Trans. Microwave Theory Tech.*, vol. 38, pp. 1433–1437, Oct. 1990.

[2] M. Davidovitz, "Calculation of multiconductor microstrip line capacitances using the semidiscrete finite element method," *IEEE Microwave Guided Wave Lett.*, vol. 1, pp. 5–7, Jan. 1991.

[3] P. H. Harms, C. H. Chan, and R. Mittra, "Modeling of planar transmission line structures for digital circuit applications," *Arch. Elek. Übertragung.*, vol. 43, pp. 245–250, 1989.

[4] W. T. Weeks, "Calculation of coefficients of capacitance multiconductor transmission lines in the presence of a dielectric interface," *IEEE Trans. Microwave Theory Tech.*, vol. MTT-18, pp. 35–43, Jan. 1970.

[5] T. G. Bryant and J. A. Weiss, "Parameters of microstrip transmission lines and of coupled pairs of microstrip lines," *IEEE Trans. Microwave Theory Tech.*, vol. MTT-16, pp. 1021–1027, Dec. 1968.

[6] R. Mittra and O. Ramahi, "Absorbing boundary conditions for the direct solution of partial differential equations arising in electromagnetic scattering problems," in *PIER 2 Finite Element and Finite Difference Methods in Electromagnetic Scattering*, M. A. Morgan, Ed. New York: Elsevier, 1990.


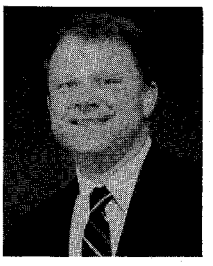

**Richard K. Gordon** (S'89–M'90) was born in Birmingham, AL, on November 26, 1959. He received the B.S. degree in physics from Birmingham-Southern College in 1983, and the M.S. degree in applied mathematics and the Ph.D. degree in electrical engineering from the University of Illinois at Urbana–Champaign in 1986 and 1990, respectively.

From May 1987 to August 1990 he worked as a Research Assistant for Prof. Raj Mittra in the Electromagnetic Communications Laboratory at the University of Illinois. In August 1990 he was appointed Assistant Professor in the Department of Electrical Engineering at the University of Mississippi, Oxford. His research interests include the use of partial differential approaches for the solution of open-region and closed-region problems in electromagnetics, numerical techniques, and the mathematical methods of electromagnetics.

Dr. Gordon is a member of Phi Kappa Phi, Phi Beta Kappa, and Eta Kappa Nu.

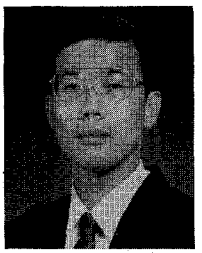

**Set Hin Fook** received the B.S. degree from the University of Malaya, Malaysia, in 1989, and the M.S. degree in electrical engineering from the University of Mississippi in 1990.

In 1989 he worked as a Quality Control Engineer at an electronic manufacturing plant. During his Master's study, he was a Research Assistant in the Department of Electrical Engineering, University of Mississippi. He currently holds the position of Operation Executive at Gravel Equipment & Supply, Inc., Amory, MS.